ORIGINAL ARTICLE

Eco-friendly Chebulic Myrobalan-Derived Porous Carbon Employed as an Electrocatalyst for the Production of Hydrogen

Raji Atchudan[1] · Suguna Perumal[2] · Ashok K. Sundramoorthy[3] · Devaraj Manoj[4,5] · Raju Suresh Kumar[6] · Abdulrahman I. Almansour[6] · Sambasivam Sangaraju[7] · Wonmok Lee[2] · Yong Rok Lee[1]

Abstract

The growing energy demand and environmental issues have encouraged the development of novel and sustainable energy. Hydrogen is one of the cleanest and most sustainable energy sources that provides an environmentally friendly alternative future fuel. The recent development in hydrogen production through electrocatalytic water-splitting is somewhat high-performance. The potential electrocatalysts play an essential role in hydrogen evolution reactions (HER) for electrochemical water splitting, where expensive and low-abundance platinum-based materials are the standard catalysts for HER. Herein, metal-free, low-cost, and naturally abundant chebulic myrobalan was employed as a source for the preparation of porous carbon by direct pyrolysis route, and the resulting porous carbon was utilized as an electrocatalyst for the production of hydrogen gas. The various analytical techniques confirmed the existence of sulfur, nitrogen, and oxygen in the prepared chebulic myrobalan-derived porous carbon (CM-PC). The presence of effective heteroatoms in the CM-PC may lead to interactive effects between the heteroatoms and porous carbon structures; this suggests the enhancement of the electrochemical performance of HER. The surface area of CM-PC was obtained as $675 \text{ m}^2 \text{ g}^{-1}$ by BET measurement. The CM-PC exhibited a moderate degree of graphitization with hydrophilic functionalities. Based on these excellent properties, the CM-PC was used as an electroactive material to fabricate the working electrode and as a metal-free electrocatalyst for HER in a 0.5 M H_2SO_4 aqueous solution. The resulting CM-PC delivered a superior catalytic activity toward HER with a Tafel slope of ~ 79 mV decade^{-1} (Overpotential $- 166$ mV$_{RHE}$ at a current density of $- 10$ mA cm^{-2}) and excellent long-term stability in an acidic medium. Importantly, these findings prove that the chebulic myrobalan (biomass) was turned into an effective electrocatalyst for hydrogen generation in the economical route, thereby challenging the uniqueness of platinum catalysts in the hydrogen economy. The result indicates that as-prepared catalysts (CM-PC) have excellent application value in energy and environment.

Keywords Chebulic myrobalan · Biomass · Pyrolysis · Porous carbon · Electrocatalyst · Hydrogen fuel · Clean energy

Raji Atchudan, Suguna Perumal, Ashok K. Sundramoorthy, and Devaraj Manoj have contributed equally to this work.

✉ Raji Atchudan
   atchudanr@yu.ac.kr

✉ Yong Rok Lee
   yrlee@yu.ac.kr

1 School of Chemical Engineering, Yeungnam University, Gyeongsan 38541, Republic of Korea

2 Department of Chemistry, Sejong University, Seoul 143747, Republic of Korea

3 Department of Prosthodontics, Saveetha Dental College and Hospitals, Saveetha Institute of Medical And Technical Sciences, Poonamallee High Road, Velappanchavadi, Chennai, Tamil Nadu 600077, India

4 Department of Chemistry, Karpagam Academy of Higher Education, Coimbatore, Tamil Nadu 641021, India

5 Centre for Material Chemistry, Karpagam Academy of Higher Education, Coimbatore, Tamil Nadu 641021, India

6 Department of Chemistry, College of Science, King Saud University, P.O. Box 2455, Riyadh 11451, Saudi Arabia

7 National Water and Energy Center, United Arab Emirates University, Al Ain 15551, United Arab Emirates

Introduction

There are several environmental crises and issues that have occurred due to the quick increase in global energy consumption. Hence, many research works are dedicated to exploring effective alternative sources and technologies. Hydrogen gas is one of the most promising clean and safe energy carriers to replace fossil fuels owing to its renewability, zero carbon releases with the advantages of eco-friendly products, and excellent energy conversion with storage features [1–6]. Interestingly, high purity with large-scale hydrogen production has been developed through electrochemical water splitting, representing a carbon–neutral and environmentally sustainable protocol [7, 8]. Thus, developing an efficient electrocatalyst with high durability is urgently needed to achieve real-time applications of energy-efficient hydrogen evolution reaction (HER) via water splitting. In recent times, carbon-based materials received broad attention for being designated as electrocatalysts for HER because of their flexible carbon substructure, abundance, and great tolerance to a broad range of pH environments, although platinum has been recognized as a benchmark HER catalyst up to now [9–11]. Advancement in carbon nanostructures has also activated their possibility as metal-free catalysts in energy conversion technologies. Among the carbon materials, porous carbon has been recognized as a promising electrocatalyst because of its large surface area with massive porosity that can offer clear paths for fast mass diffusion, excellent electrical conductivity, and electrochemical stability [2, 3]. In addition, the proper amount of heteroatoms such as nitrogen, phosphorous, sulfur, and boron doping in porous carbon materials significantly improves its electrocatalytic activity through a synergistic effect [12]. Particularly, nitrogen atoms in the carbon matrix can effectively enhance the catalytic active site and electrocatalytic activity of the carbon material due to their tunable electronic properties, high stability, anticorrosion, and conductivity [2, 3, 13]. Multiple heteroatom-doped carbon material displays the smallest Gibbs free energy of hydrogen adsorption compared to single heteroatom-doped carbon material, which endorses much higher HER activity under acid and alkaline conditions for the reason that of the synergetic effect [14]. Various heteroatom-based synthetic precursors have been used to introduce heteroatoms into carbon-based materials to improve their electrocatalytic activities. Nevertheless, synthetic compounds are harmful to humans and to the environment as well, also they are expensive [5, 6]. Therefore, finding a simple, cheap, green heteroatom especially a nitrogen/sulfur-containing precursor to prepare nitrogen/sulfur-codoped

carbon-based materials is essentially needed. In general biomass/ biowaste green resources (such as walnut shell, peanut shells, broccoli stem, corn stalks, food waste, palm waste, bean sprouts, cashew nut-skin waste, lotus seedpod, lotus stem, banana peel, and so on) have been confirmed the presence of many phytoconstituents which results in heteroatom-doped porous carbon materials [10, 10, 11, 11, 15–22]. These biomass derived porous carbon materials showed comparatively higher robust catalytic activity and long-term stability towards HER in alkaline and acidic mediums.

The use of biomass not only gives hetero atom-enriched carbon materials but also it reduces pollution. Methods, including the enzymatic hydrolysis route, hydrothermal process, and or pyrolysis route, are available for the preparation of heteroatom-doped porous carbon from biomass [23–25]. Among the above methods, pyrolysis technology is widely used for recycling biomass/biowaste due to their unique characteristics of converting low-value biomass into high-value energy products (comparatively straightforward method, high energy conversion efficiency, and short reaction duration with quality products) [26, 27]. To increase heteroatom-enriched biomass utilization value, the development of a pyrolysis route based on biomass's unique elemental composition to maximize the enrichment of target elements is still in investigation.

Inspired by the above findings, we used the chebulic myrobalan (CM) as a biomass source for the synthesis of chebulic myrobalan-derived porous carbon (CM-PC) material. Also, we rely on the fact that as CM-PC material is from plant sources, it will have abundant heteroatoms and may have outstanding electrocatalytic activity. Besides, CMs are easily available and environmentally friendly precursors in Asia. The CM can help to astringe the body tissues, which may help to treat diarrhea and hemorrhoids. This herb's cold and dry qualities may also help relieve inflammation and soothe irritated skin. Various state-of-the-art characterization techniques determined the physicochemical properties including structural, chemical composition, and morphological features of as-prepared CM-PC material. After careful characterization, CM-PC was used as an active catalytic material for the fabrication of a working electrode. Then, the electrocatalytic performances of the fabricated electrocatalysts including linear sweep voltammetry (LSV), basics of electrochemical impedance spectroscopy (EIS), and long-term durability were studied for HER in an acidic medium (0.5 M H_2SO_4 aqueous solution). Further, the electrochemical reaction and stability of the CM-PC were discussed. The results obtained from HER were compared with already reported materials in order to show the superiority of the CM-PC material.

Scheme 1. Formation of biomass-based porous carbon materials by simple pyrolysis under constant nitrogen gas flow and its application for hydrogen production
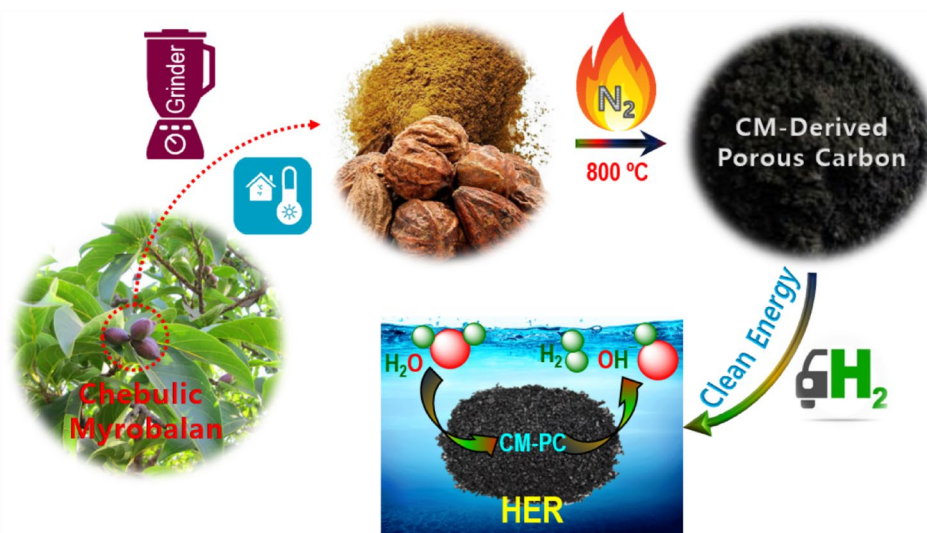
Experimental

Preparation of Porous Carbon Material from Chebulic Myrobalan

The biomass-derived porous carbon material was prepared through a pyrolysis method using dried CM fruit. In a typical procedure, the dried CM fruit was first pounded into a powder using a commercial mixture grinder. Then the milled raw material was transferred to a quartz boat, placed at the center of the quartz tube in the tubular furnace, and heated to 800 °C with a ramp rate of 10 °C min^{-1}. The temperature was maintained for 3 h under a continuous nitrogen protective environment and after the reaction time, the furnace was cooled to room temperature. The resultant carbon product was ground using a mortar and pestle. Finally, the obtained biomass-derived CM-PC material was investigated by various physicochemical characterizations to determine its structural and electrochemical properties. The detailed CM-PC material synthesis procedure and its applications were demonstrated in Scheme 1.

Results and Discussion

Structural Properties of Synthesized Porous Carbon Material

Naturally abundant CM was employed as a dual source for the preparation of heteroatoms interconnected porous carbon by direct pyrolysis route and investigated by various measurements. The morphologies of the CM-PC electrocatalyst were examined by the field emission-scanning electron microscope (FE-SEM) and field emission-transmission electron microscope (FE-TEM). As shown in Fig. 1a and

b, the CM-PC demonstrates a stacked 2D sheet-like layer structure with smooth surface morphology, and folds are observed on the carbon surfaces and edges. The dimensions range of CM-PC materials are from hundreds of nanometers to several micrometers. The high-resolution images (Fig. 1c and d) display irregular pores with uniform distribution. The internally interconnected pores speared through the entire carbon matrix. The formation of interconnected pores in the CM-PC is credited to the unstable phytoconstituent escaping from the biomass (CM) during the pyrolysis. The chemical (elemental) compositions of CM-PC were determined from FE-SEM-energy dispersive X-ray (EDX) spectral and elemental mapping data. Figure 1e–i shows the FE-SEM electron image and corresponding element mapping images of CM-PC. FE–SEM–EDX elemental mapping images demonstrated that the CM-PC had carbon, oxygen, nitrogen, and sulfur elements with uniform distribution. Moreover, the overlapping of FE–SEM–EDX element mapping images (Fig. S1a) further validates the presence of oxygen, nitrogen, and sulfur elements over the carbon matrix. The FE–SEM–EDX spectrum of CM-PC additionally confirms the chemical composition and purity of CM-PC. The FE–SEM–EDX spectrum (Fig. S1b) demonstrated that the CM-PC possessed carbon, oxygen, nitrogen, and sulfur elements, which are from the source material CM. Apart from these crucial elements, the FE–SEM–EDX spectrum shows silicon and platinum peaks that originated from the silicon wafer (substrate) and coating, respectively, that are used for the microscopic analysis.

The porous characteristics with crystallization/graphitization of the CM-PC can be viewed directly by FE-TEM with selected area electron diffraction (SAED), and the corresponding results are displayed in Fig. 2. TEM images (Fig. 2a and b) confirm the high porous network. Moreover, these interconnected porous structures of CM-PC are
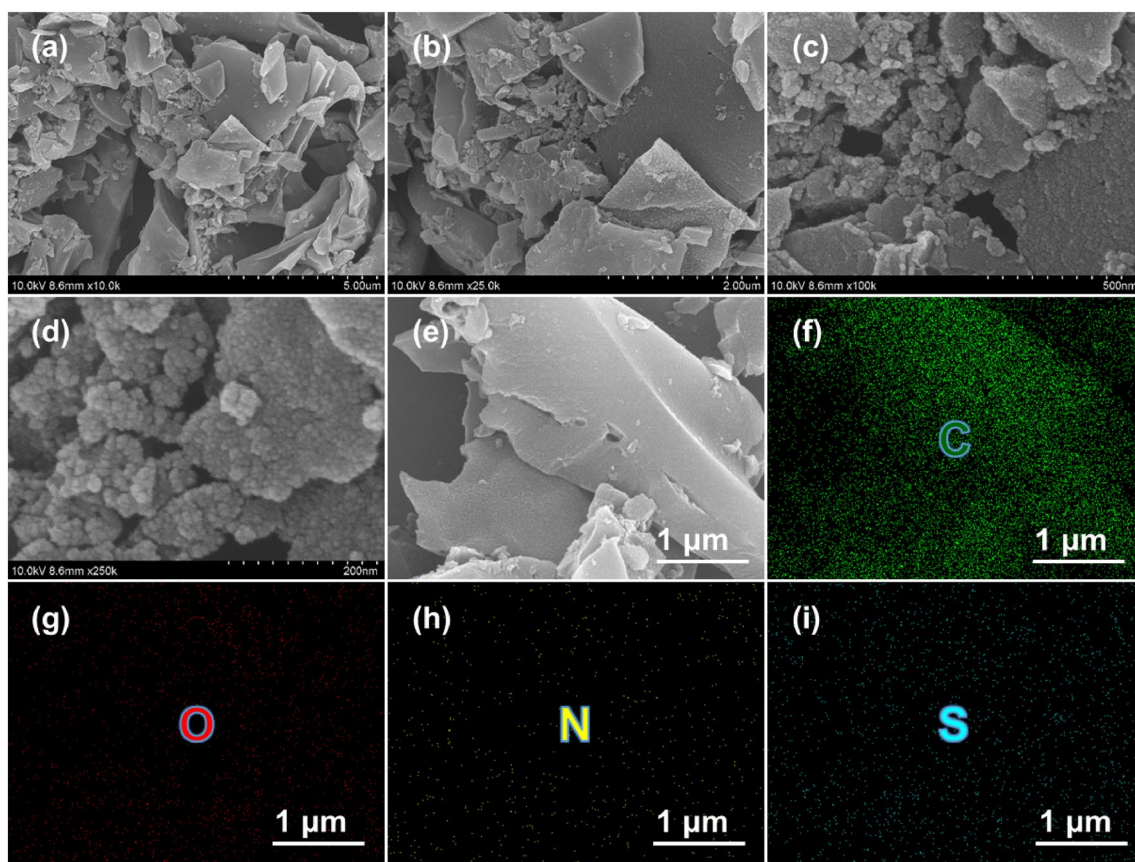
Fig. 1 Surface morphology of prepared porous carbon. **a–e** FE-SEM image of the obtained CM-PC and **f–i** Corresponding elemental mapping images of carbon, oxygen, nitrogen, and sulfur atoms

assumed to have a favorable penetration of the electrolyte (quick transport of electron) and could shorten the pathways between electrode and electrolyte that sufficiently may improve the diffusion of electrolyte from the pores. This is significant for fast charge–discharge of the electrode [28]. Figure 2c and d demonstrate that the high-magnification TEM images of the CM-PC reveal partial graphitization; hence, the CM-PC might have good electric conductivity [29]. The insets in Fig. 2d show the SAED patterns of the CM-PC and exhibit some narrow rings assigned to diffraction patterns.

The X-ray diffraction (XRD) profile and Raman spectrum revealed information about the phase structures, including phase purity and degree of crystallinity/graphitization of porous carbon materials. The wide-angle powder XRD of CM-PC (Fig. 3a) displayed broad and distinct peaks centered at ($2\theta =$) 23.5 and 43.5°, which can be indexed to the (0 0 2) and (1 0 0) planes that are responsible for the typical carbon materials [30–33]. Broad peaks rather than sharp peaks suggest that the partial graphitization of CM-PC (low degree of crystallinity) is due to its surface functionalization during thermal annealing (pyrolysis). Also, the broad peaks indicate that the center-to-center spacings of the mesopores

have relatively wide distributions [28]. Raman spectrum of CM-PC (Fig. 3b) shows two distinct peaks centered at 1590 and 1345 cm^{-1} corresponding to the ordered graphitic structures (sp^2-hybridized carbon atoms, G band) and disordered domains (sp^3-hybridized carbon atoms, D band), respectively [34, 35]. The intense D band suggests that the CM-PC had a moderate degree of graphitization. Additionally, a weak and broad peak centered at 2850 cm^{-1} corresponds to the 2D band, which reveals partial graphitization (moderate degree of graphitization).

Furthermore, the intensity ratio of "D band" and "G band" (I_D/I_G) has been calculated which was less than one, indicating the partial graphitization of CM-PC [36], which might result in good electric conductivity. The XRD and FE-TEM results are in good agreement that CM-PC has partial graphitization/crystallization.

The surface area and pore nature of the carbon material plays a crucial role in electrochemical reaction performance. Thus the porosity of CM-PC has been investigated by nitrogen adsorption and desorption experiments. Figure 4a displays the nitrogen adsorption–desorption isotherms of CM-PC. Nitrogen isotherms demonstrate that the CM-PC are likely both type I and type IV isotherms with an H-4

Fig. 2 Morphology of prepared porous carbon. **a**, **b** TEM image of the obtained CM-PC and **c**, **d** FE-TEM image of the obtained CM-PC (inset (**d**): FE-TEM-SAED pattern of CM-PC)
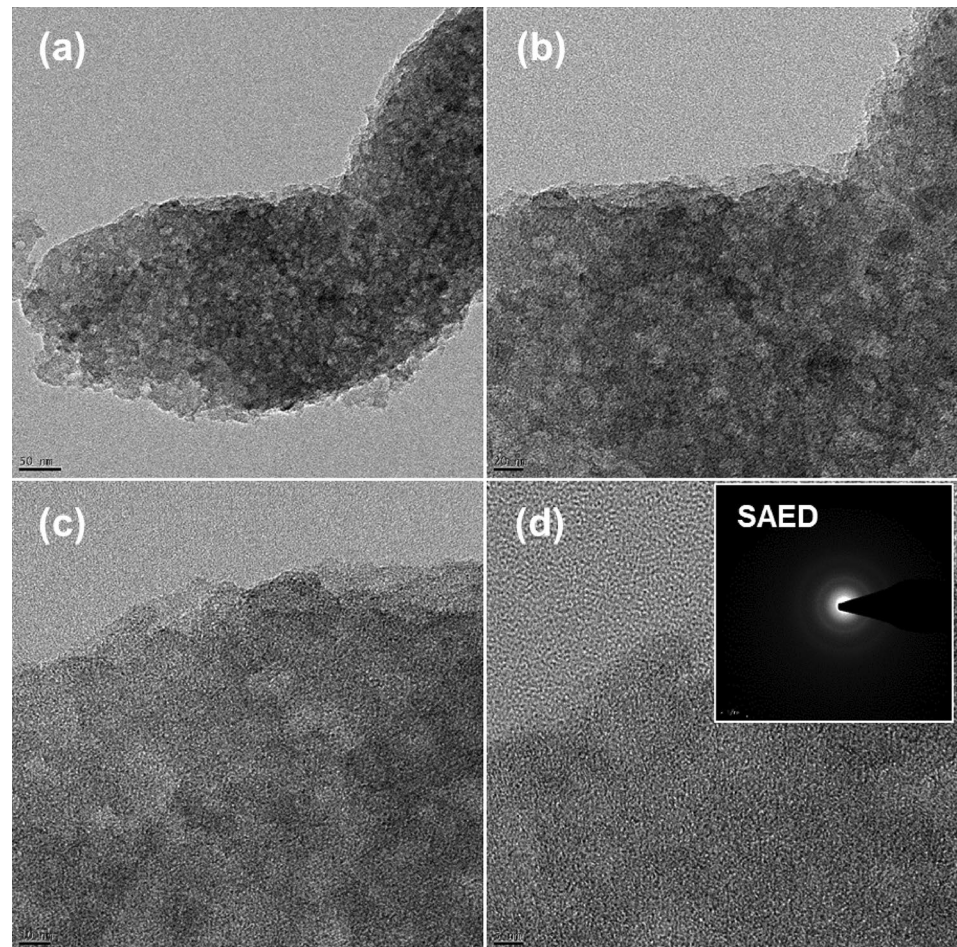

Fig. 3 **a** XRD profile and **b** Raman spectrum of the obtained CM-PC
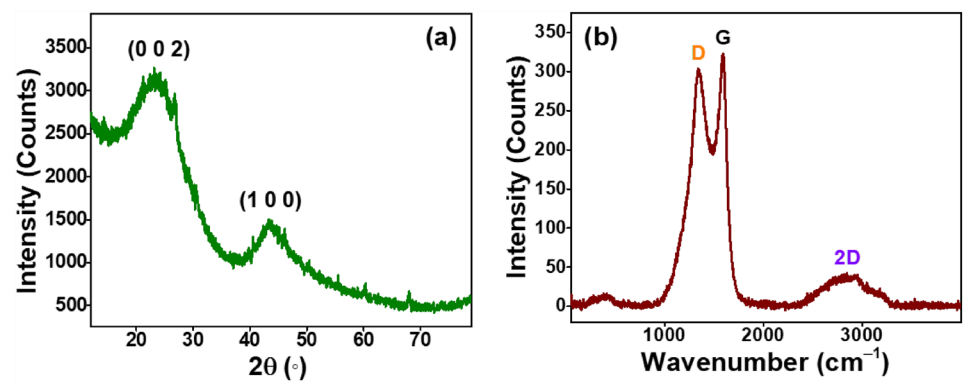
hysteresis loop based on IUPAC classification, indicating the micropores and mesopores in the CM-PC [37–40]. A steep rise was observed in the isotherms at the low relative pressure (P/P$_0$ < 0.1), corresponding to higher nitrogen uptake in the micropores [41]. The clear hysteresis loop (0.1 < P/P$_0$ < 1.0) and a little sharp rise in the nitrogen isotherms at high relative pressure (P/P > 0.9) suggest the existence of mesopores and macropores in the CM-PC [32, 33, 42]. The small number of macropores may originate from the accumulation of carbon particles/sheets. The nitrogen adsorption

and desorption experiments revealed that CM-PC has a surface area of ~650 m^2 g^{-1} using the Brunauer–Emmet–Teller (BET) method. This high surface area with porosity might enhance the electrochemical properties of CM-PC towards HER [43].

Chemical functional information of the CM-PC was obtained by attenuated total reflection (ATR)-Fourier transform infrared (FTIR) spectroscopy. The stretching vibration of N–H and C–H bonds appeared at 3330 and 2950 cm^{-1}, respectively [44, 45]. In general, biomass exhibits good C–H
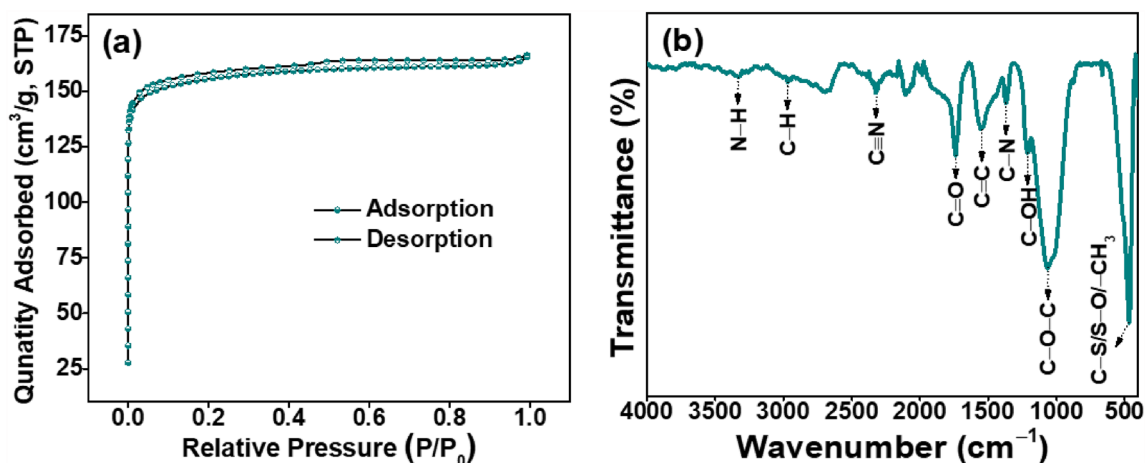
Fig. 4 **a** Nitrogen adsorption–desorption isotherms and **b** ATR—FTIR profile of the obtained CM-PC

bond stretching, but the C–H bond intensity is insignificant in CM-PC; it might be broken during the pyrolysis process to form a more stable C=C (sp^2-hybridized carbon) bond that was observed at 1560 cm^{-1} [46]. The small absorption band observed at 2323 cm^{-1} suggests the presence of C≡N stretching vibration. The IR spectrum of CM-PC displayed more obvious absorption bands at around 1737, 1370, 1212, and 1060 cm^{-1}, which credits to the C=O in carbonyl groups, C–N in the carbon matrix, O–H in the carboxyl groups and C–O in epoxy groups, respectively [47, 48]. The bands around 1560 and 1060 cm^{-1} observed spectrum indicate the presence of a C=C (from the aromatic ring) and C–O–C stretching, respectively [49, 50]. The minor peak at 668 cm^{-1} corresponds to N–H out-of-plane deformation vibration [51]. The strong absorption band at around 470 cm^{-1} is assigned to the C–S (sulfur bonded with carbon matrix)/S–O (oxidized sulfur)/–CH$_3$ out-plane stretching on aromatic carbon functional groups. This result confirms that the prepared CM-PC has successful incorporation of nitrogen-, oxygen-, and sulfur-containing functional groups.

The X-ray photoelectron spectroscopy (XPS) technique was employed to determine the elemental composition of prepared CM-PC. As shown in Fig. S2, the survey spectrum of CM-PC contains two prominent and two minor peaks at the binding energy level of 164, 284, 431, and 532, corresponding to sulfur, carbon, nitrogen, and oxygen, respectively. The XPS elemental analysis revealed for 80% carbon, 16% oxygen, and small quantities of nitrogen (3%) and sulfur (1%). Figure 5a displays high-resolution XPS spectra of C 1 s level exhibiting a broad peak which has been deconvoluted into four peaks at the binding energies of 283.9, 284.6, 285.6, and 286.7 eV that are attributed to the signals of hydrogen-bonded carbon (–C–H), graphitic sp^2 bonded carbon (C=C)/sp^3 bonded carbon (C–C), ether/alcohol (C–O–C/C–OH)/C–N/C–S functionalities, and

ketone/aldehyde/carboxyl (C=O/–CHO/HO–C=O) groups, respectively [15–17, 52–54]. The presence of a graphitic sp^2-hybridization (C=C bond), along with other C–C and C–O functionalities in the CM-PC, advises for advanced electric conductivity [55]. The existence of C–N, and C–S bonds confirms that the carbon matrix of CM-PC is doped with nitrogen and sulfur. The high-resolution spectrum of O 1 s was used to investigate the nature of oxygen species. The O 1 s spectrum (Fig. 5b) of CM-PC can be divided into three distinct peaks in the binding energy level of 531.0, 532.5, and 533.6 eV attributed to the carbonyl groups (C=O), epoxy/hydroxyl groups (C–O–C/C–OH) and carboxyl groups (HO–C=O), respectively [23–25, 56, 57]. The high-resolution spectrum of N 1 s was used to examine the nature of nitrogen species. Figure 5c displays the N 1 s excitation of CM-PC was deconvoluted into three typical component peaks namely; pyridinic-N groups (C–N–C, 398.5 eV), pyrrolic-N groups (C–N–H, 400.9 eV), and quaternary-N groups (C$_3$–N, 403.6 eV), respectively. The presence of pyridinic-N, pyrrolic-N, and quaternary-N is believed to readily promote the surface wettability of electrode material by electrolyte, which subsequently improves the electrochemical properties of CM-PC towards HER [18, 58]. Figure 5d shows the deconvoluted S 2p for the CM-PC with spectrum peaks centered at 162.5, 164.6, and 168.8 eV, which corresponds to the S 2p$_{3/2}$ spin–orbit splitting (–C–S–), S 2p$_{1/2}$ spin–orbit splitting (–C–S–), and the possibility of sulfur is bonded with both nitrogen and oxygen species in the carbon matrix (–S–N/–S–O/C–SO$_3$–), respectively [15–17, 59, 60]. The above characterization results confirm that the prepared CM-PC has partial graphitization with adequate pores and successful incorporation of nitrogen-, oxygen-, and sulfur-containing functional groups. Based on these excellent properties, the electrochemical performance of the CM-PC towards HER is expected to be significantly improved.

Fig. 5 XPS analysis of prepared porous carbon. High-resolution XPS spectra of **a** C 1 s, **b** O 1 s, **c** N 1 s, and **d** S 2p excitation levels
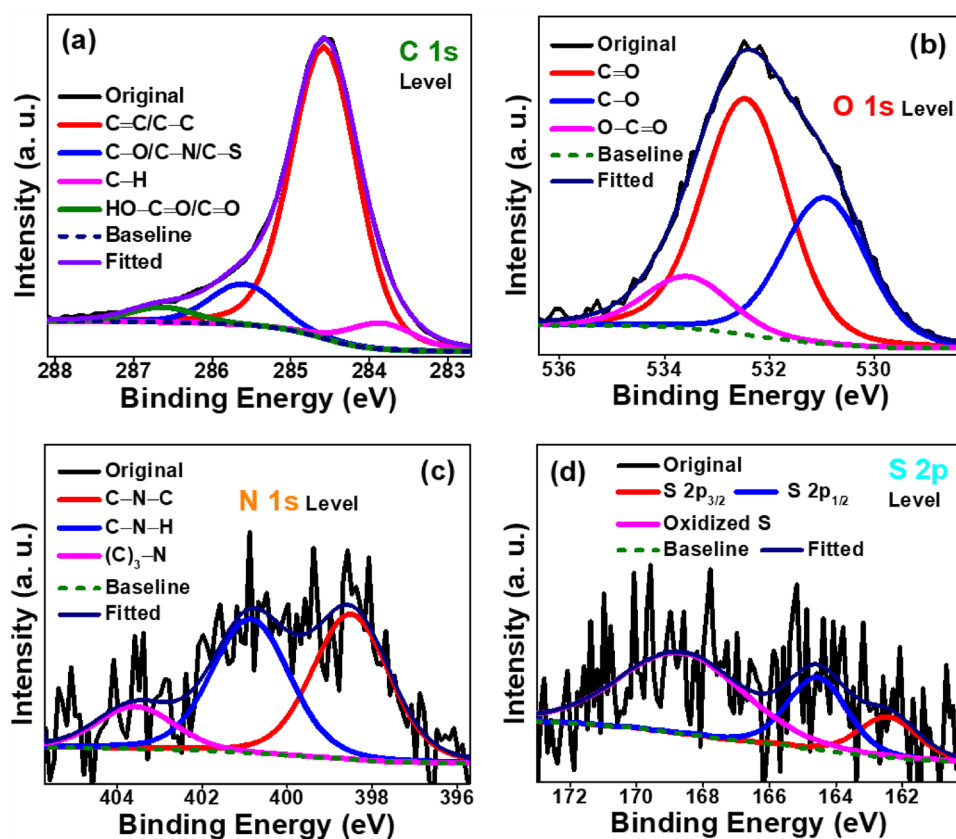

Electrochemical Properties of Synthesized Porous Carbon Material

In order to measure the electrochemical performance of the CM-PC material towards HER, LSV measurements were conducted using a three-electrode cell configuration in 0.5 M H_2SO_4 aqueous electrolyte. Figure 6a displays the LSV polarization curves with iR correction on a reversible hydrogen electrode (RHE) scale of CM-PC loaded carbon cloth, pristine carbon cloth, and bare platinum plate (1 cm^2) at a sweep rate of 10 mV s^{-1} under the same conditions. The cathodic current density of the pristine carbon cloth does not change much with the increase of negative potential. Not surprisingly, the pristine carbon cloth shows an overpotential -800 mV vs. RHE at -10 mA cm^{-2}, which is a higher potential value compared to other electrode materials. Therefore, pristine carbon cloth showed the lowest (negligible) HER activity than the other electrode materials. The cathode current density of the prepared CM-PC material increased rapidly with the increase of negative potential suggesting that the synthesized CM-PC material had good catalytic activity [10, 11, 43, 61]. The overpotential values for CM-PC material and the bare platinum plate are -166 and -45 mV vs. RHE at -10 mA cm^{-2}, respectively. LSV polarization curves of CM-PC and bare platinum plate show similar trends by HER overpotential and ultimate current

density being close. These LSV profile results indicate that the catalytic activity of CM-PC material is much greater than that of pristine carbon cloth but lower than the bare platinum plate. These excellent catalytic activities are due to the synergistic interaction between successfully incorporated heteroatoms (nitrogen and sulfur) with carbon matrix in CM-PC materials. Tafel slope is one of the valuable parameters for the evaluation of the electrocatalyst's performance towards HER. A smaller Tafel slope generally denotes faster hydrogen production increase with potential increase. Tafel slopes (plots) of resulting electrocatalysts were obtained from the corresponding LSV curves by proper fitting, which is presented in Fig. 6b. The Tafel slopes of pristine carbon cloth, CM-PC material loaded carbon cloth, and bare platinum plate were 285 mV decade^{-1}, 79 mV decade^{-1}, and 38 mV decade^{-1}, respectively. The obtained Tafel slope value of CM-PC material was much lower than that of pristine carbon cloth, suggesting that the CM-PC material owns the fastest hydrogen production [10, 11]. However, the Tafel slope value of CM-PC material is higher than that of the bare platinum plate. The excellent catalytic performance of CM-PC material might be due to various factors such as (i) a perfect spongy-like two-dimensional structure with abundant active sites during the catalytic process; (ii) rich porous structure beneficial for the diffusion of electrolyte and the release of evolved hydrogen; (iii) the heteroatom (especially nitrogen)

Fig. 6 Electrochemical analysis of prepared porous carbon. **a** LSV polarization profiles obtained at 10 mV s^{-1}, **b** Tafel slope, **c** EIS Nyquist plots, the inset-diagram is a suitable equivalent circuit, and **d** Durability test of CM-PC material in 0.5 H_2SO_4 aqueous electrolyte
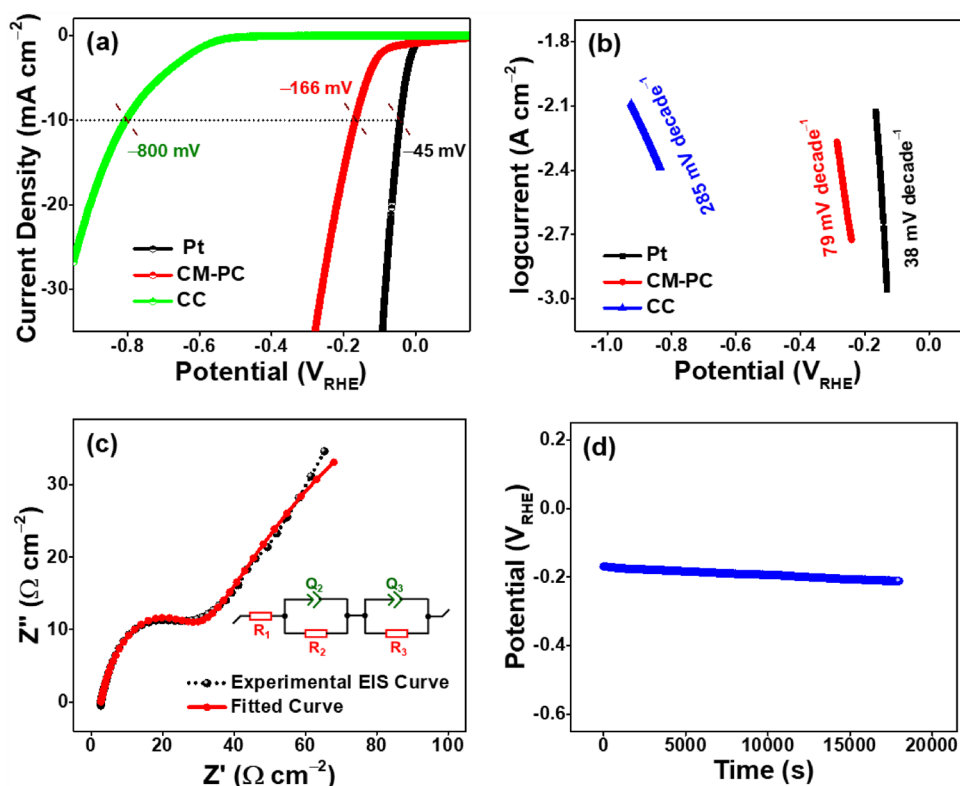
doping in the CM-PC material could prevent the aggregation also alleviate the conductivity [62]. In order to show the superiority of the current materials, the electrocatalytic performance of CM-PC material for HER correlates with the other related materials reported in the recent literature. Table 1 [10, 11, 18, 23–25, 61, 63–65] shows the comparison overpotential values at − 10 mA cm^{-2} and Tafel slopes. Interestingly, the electrocatalytic activity of CM-PC material for HER is higher than the other biomass-derived carbon materials. However, CM-PC showed slightly less activity than cashew but still, the values are comparable.

The HER pathways in acidic media were most commonly divided into three possible reaction steps. In the HER mechanism, the first step (1) is the Volmer reaction step

(electrochemical adsorption of hydrogen ions). The second step (2) is known as the Heyrovsky reaction. Here, the hydrogen evolution reaction can proceed (electrochemical desorption reaction). Finally, the Tafel's reaction step (3). Both the Heyrovsky reaction step and the Tafel reaction step produce H_2 [5, 6, 10, 11, 66].

$$H^+ + e^- \leftrightarrow H_{ad}, \tag{1}$$

$$H^+ + e^- + H_{ad} \leftrightarrow H_2, \tag{2}$$

$$2H_{ad} \leftrightarrow H_2. \tag{3}$$

Table 1 Comparison of HER activity of prepared CM-PC material with other reported biomass-derived electrocatalysts

Biomass (Source)	Electrolyte Solution	Overpotential at − 10 mA cm^{-2}	Tafel slope (mV decade^{-1})	References
Bean sprout	0.5 M H_2SO_4	413 mV	98	[18]
Carrot	0.1 M KOH	297 mV	135	[64]
Cattail fiber	0.5 M H_2SO_4	248 mV	135	[63]
Silk fibroin	0.5 M H_2SO_4	138 mV	168	[61]
Cashew	0.5 M H_2SO_4	133	75	[16]
Silk fabric	0.5 M H_2SO_4	336 mV	311	[23–25]
Palm waste	0.5 M H_2SO_4	330 mV	63	[10, 11]
Banana fibers	0.5 M H_2SO_4	332	161	[65]
Chebulic myrobalan	0.5 M H_2SO_4	166	79	This work

Electrochemical impedance spectroscopy (EIS) measurement in the electrochemical process significantly influences the catalytic reaction. Thus, the EIS measurement was performed in an acidic aqueous solution to confirm the rapid electron transfer ability of CM-PC material. The EIS Nyquist plot of CM-PC material is shown in Fig. 6c. In general, the high-frequency region in the EIS spectrum is significantly associated with the porous nature of the active electrode material [67]. The low-frequency region is mainly associated with the overpotential used, which reflects the size of the charge transfer resistance. The charge transfer resistance is also related to the rate of catalytic reaction [68]. The EIS Nyquist plots displayed that CM-PC material has the minor diameter of a semicircle arc, implying it had little charge transfer resistance during the HER process. The little charge transfer resistance is beneficial for enhancing electrocatalysis behaviors of hydrogen evolution, which has fast electron transfer. Also, the HER rate is quicker and further reflects its outstanding catalytic activity. Long-term durability is also one of the essential parameters for the prepared CM-PC material in practical applications. The chronopotentiometric curve in Fig. 6d demonstrates that CM-PC material had remarkable stability with continued HER activity for 18,000 s (5 h) at a constant current density of -10 mA cm^{-2}. This implies biomass-based CM-PC material with a great application value for HER in an acidic medium.

After stability measurement, the LSV polarization profile was recorded and compared with the initial LSV polarization profile to further prove the electrochemical stability of the prepared catalysts towards HER in the acidic medium. As shown in Fig. 7a, the LSV polarization profiles of CM-PC material in 0.5 H$_2$SO$_4$ aqueous electrolyte before and after long-term durability (18,000 s) at a constant current density of -10 mA cm^{-2} are compared. After long-term durability, the LSV polarization profile really matches well with the initial LSV polarization curve. The result demonstrated that the CM-PC material electrocatalytic activity of hydrogen evolution without any noticeable weakening suggests excellent long-term stability. In order to confirm the electrochemical

stability of the prepared electrocatalyst, the EIS measurement was also conducted for the CM-PC material before and after the stability measurement. The corresponding EIS Nyquist plots were compared to each other, as shown in Fig. 7b. After stability measurement, the EIS Nyquist plot of CM-PC material shows an insignificant deviation from the initial EIS Nyquist plot. The insignificant changes of EIS Nyquist semicircle art imply the interfacial charge transfer resistance and mass transport through the porous nature of the CM-PC material retained even after long-term durability. Overall, the results above confirm the superior electrocatalytic activity and durable stability of prepared CM-PC material in acidic electrolytes.

Conclusions

An environmentally friendly, efficient, and cost-effective CM-PC material has been successfully prepared using earth-abundant CM as a precursor through a thermal pyrolysis route. This strategy possesses excellent promise for implementation due to the low cost of precursor and facile process. The obtained CM-PC was characterized through various physicochemical techniques, such as FE–SEM–EDX, FE–TEM, XRD, Raman, nitrogen sorptions, ATR-FTIR, and XPS analyses. The above characterization techniques revealed that the as-prepared CM-PC has partial graphitization, high surface area with adequate pores, and with oxygen-, nitrogen-, and sulfur-existing functionalities, which were highly favored for the electrochemical reaction. The as-prepared CM-PC was directly used for the fabrication of a working electrode (electrocatalyst) for HER without any additional processes. Thus, the HER based on ideal CM-PC delivers an attractive overpotential of -166 mV at -10 mA cm^{-2} with a lower Tafel slope of 79 mV decade^{-1} and excellent stability in 0.5 M H$_2$SO$_4$ aqueous solution. The results showed that the biomass (CM)-derived porous carbon could be applied as a catalyst for HER in an acidic medium. Furthermore, this approach can be extended to prepare

Fig. 7 Electrochemical analysis of prepared porous carbon. **a** LSV polarization curves obtained before and after long-term durability at 10 mV s^{-1}, and **b** EIS Nyquist plots obtained before and after long-term durability of CM-PC material in 0.5 H$_2$SO$_4$ aqueous electrolyte
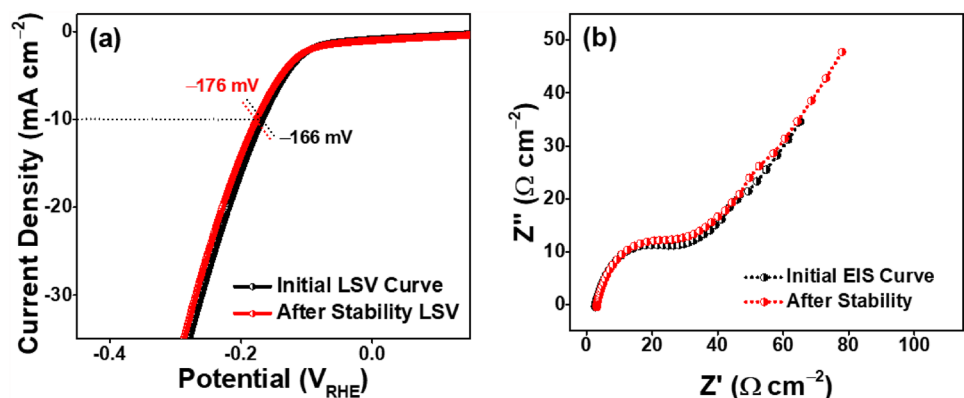
diverse biomass-derived porous carbon materials using different biomass/biowaste precursors. Also, it might offer great benefits for the mass production of biomass-derived porous carbon materials for advanced energy harvesting.

References

1. Y. Dou, A. Wang, L. Zhao, X. Yang, Q. Wang, M. Shire Sudi, W. Zhu, D. Shang, Boosted hydrogen evolution reaction for a nitrogen-rich azo-bridged metallated porphyrin network. J. Colloid Interface Sci. **650**, 943 (2023)

2. M. Sun, S. Yun, J. Dang, Y. Zhang, Z. Liu, D. Qiao, 1d/3d Rambutan-like Mott–Schottky porous carbon polyhedrons for efficient tri-iodide reduction and hydrogen evolution reaction. Chem. Eng. J. **458**, 141301 (2023)

3. Z. Sun, T. Wang, R. Zhang, H. Li, Y. Wu, S. Toan, Z. Sun, Boosting hydrogen production via deoxygenation-sorption-enhanced biomass gasification. Biores. Technol. **382**, 129197 (2023)

4. A. Wang, Y. Dou, X. Yang, Q. Wang, M.S. Sudi, L. Zhao, D. Shang, W. Zhu, J. Ren, Efficient oxygen evolution reaction from iron-molybdenum nitride/molybdenum oxide heterostructured composites. Dalton Trans. **52**, 11234 (2023)

5. N. Wang, X. Bo, M. Zhou, Laser conversion of biomass into porous carbon composite under ambient condition for pH-universal electrochemical hydrogen evolution reaction. J. Colloid Interface Sci. **604**, 885 (2021)

6. S. Wang, A. Lu, C.-J. Zhong, Hydrogen production from water electrolysis: role of catalysts. Nano Converg. **8**, 4 (2021)

7. H.-L. Huang, X. Guan, H. Li, R. Li, R. Li, S. Zeng, S. Tao, Q. Yao, H. Chen, K. Qu, Ir nanoclusters/porous n-doped carbon as a bifunctional electrocatalyst for hydrogen evolution and hydrazine oxidation reactions†. Chem. Commun. **58**, 2347 (2022)

8. S. Shenoy, C. Chuaicham, K. Sasaki, S. Park, M. Nallal, K.H. Park, K. Sekar, Nitridation-free preparation of bimetallic oxide-nitride bifunctional electrocatalysts for overall water splitting. Chem. Commun. **59**, 12454 (2023)

9. K. Pandey, H.K. Jeong, Coffee waste-derived porous carbon for hydrogen and oxygen evolution reaction. Chem. Phys. Impact **6**, 100175 (2023)

10. N. Prabu, T. Kesavan, G. Maduraiveeran, M. Sasidharan, Bio-derived nanoporous activated carbon sheets as electrocatalyst for enhanced electrochemical water splitting. Int. J. Hydrogen Energy **44**, 19995 (2019)

11. N. Prabu, R.S.A. Saravanan, T. Kesavan, G. Maduraiveeran, M. Sasidharan, An efficient palm waste derived hierarchical porous carbon for electrocatalytic hydrogen evolution reaction. Carbon **152**, 188 (2019)

12. X. Li, J. Ma, J. Luo, S. Cheng, H. Gong, J. Liu, C. Xu, Z. Zhao, Y. Sun, W. Song, K. Li, Z. Li, Porous n, p co-doped carbon-coated ultrafine CO_2P nanoparticles derived from DNA: an

13. P. Tan, Y. Wang, L. Yang, X. Zhang, J. Pan, Nitrogen-doped carbon coated Ni_3Mo_3N porous microrods as efficient electrocatalyst for hydrogen evolution reaction. Diam. Relat. Mater. **136**, 109974 (2023)

14. Y. Wang, S. Wang, R. Li, H. Li, Z. Guo, B. Chen, R. Li, Q. Yao, X. Zhang, H. Chen, Y. Li, K. Qu, Y. Zheng, A simple strategy for tridoped porous carbon nanosheet as superior electrocatalyst for bifunctional oxygen reduction and hydrogen evolution reactions. Carbon **162**, 586 (2020)

15. R. Atchudan, S. Perumal, T.N.J.I. Edison, A.K. Sundramoorthy, R. Vinodh, S. Sangaraju, S.C. Kishore, Y.R. Lee, Natural nitrogen-doped carbon dots obtained from hydrothermal carbonization of chebulic myrobalan and their sensing ability toward heavy metal ions. Sensors **23**, 787 (2023)

16. R. Atchudan, S. Perumal, T.N. Jebakumar Immanuel Edison, A.K. Sundramoorthy, N. Karthik, S. Sangaraju, S.T. Choi, Y.R. Lee, Biowaste-derived heteroatom-doped porous carbon as a sustainable electrocatalyst for hydrogen evolution reaction. Catalysts **13**, 542 (2023)

17. R. Atchudan, S. Perumal, A.K. Sundramoorthy, D. Manoj, R.S. Kumar, A.I. Almansour, Y.R. Lee, Facile synthesis of functionalized porous carbon by direct pyrolysis of *Anacardium occidentale* nut-skin waste and its utilization towards supercapacitors. Nanomaterials **13**, 1654 (2023)

18. X. Cao, Z. Li, H. Chen, C. Zhang, Y. Zhang, C. Gu, X. Xu, Q. Li, Synthesis of biomass porous carbon materials from bean sprouts for hydrogen evolution reaction electrocatalysis and supercapacitor electrode. Int. J. Hydrogen Energy **46**, 18887 (2021)

19. D. Chinnadurai, P. Karuppiah, S.-M. Chen, H.-J. Kim, K. Prabakar, Metal-free multiporous carbon for electrochemical energy storage and electrocatalysis applications. New J. Chem. **43**, 11653 (2019)

20. H.-H. Fu, L. Chen, H. Gao, X. Yu, J. Hou, G. Wang, F. Yu, H. Li, C. Fan, Y.-L. Shi, X. Guo, Walnut shell-derived hierarchical porous carbon with high performances for electrocatalytic hydrogen evolution and symmetry supercapacitors. Int. J. Hydrogen Energy **45**, 443 (2020)

21. Z. Liu, Q. Zhou, B. Zhao, S. Li, Y. Xiong, W. Xu, Few-layer n-doped porous carbon nanosheets derived from corn stalks as a bifunctional electrocatalyst for overall water splitting. Fuel **280**, 118567 (2020)

22. K.R.A. Saravanan, N. Prabu, M. Sasidharan, G. Maduraiveeran, Nitrogen-self doped activated carbon nanosheets derived from peanut shells for enhanced hydrogen evolution reaction. Appl. Surf. Sci. **489**, 725 (2019)

23. H. Zhang, K. Yang, Y. Tao, Q. Yang, L. Xu, C. Liu, L. Ma, R. Xiao, Biomass directional pyrolysis based on element economy to produce high-quality fuels, chemicals, carbon materials—a review. Biotechnol. Adv. **69**, 108262 (2023)

24. L. Zhang, D. Qin, J. Feng, T. Tang, H. Cheng, Rapid quantitative detection of luteolin using an electrochemical sensor based on electrospinning of carbon nanofibers doped with single-walled carbon nanoangles. Anal. Methods **15**, 3073 (2023)

25. W. Zhang, R. Xi, Y. Li, Y. Zhang, P. Wang, D. Hu, Waste silk fabric derived n-doped carbon as a self-supported electrocatalyst for hydrogen evolution reaction. Colloids Surf., A **658**, 130704 (2023)

26. W. Cai, X. Wang, Z. Zhu, R. Kumar, P. Nana Amaniampong, J. Zhao, Z.-T. Hu, Synergetic effects in the co-pyrolysis of lignocellulosic biomass and plastic waste for renewable fuels and chemicals. Fuel **353**, 129210 (2023)

27. S. Zhang, Y. Mei, G. Lin, Pyrolysis interaction of cellulose, hemicellulose and lignin studied by TG-DSC-MS. J. Energy Inst. **112**, 101479 (2024)

28. Z. Zhou, T. Liu, A.U. Khan, G. Liu, Controlling the physical and electrochemical properties of block copolymer-based porous carbon fibers by pyrolysis temperature. Mol. Syst. Design Eng. **5**, 153 (2020)

29. M. Chen, S. Jiang, C. Huang, X. Wang, S. Cai, K. Xiang, Y. Zhang, J. Xue, Honeycomb-like nitrogen and sulfur dual-doped hierarchical porous biomass-derived carbon for lithium–sulfur batteries. Chemsuschem **10**, 1803 (2017)

30. P. Cheng, T. Li, H. Yu, L. Zhi, Z. Liu, Z. Lei, Biomass-derived carbon fiber aerogel as a binder-free electrode for high-rate supercapacitors. J. Phys. Chem. C **120**, 2079 (2016)

31. S. Karthikeyan, G. Sekaran, In situ generation of a hydroxyl radical by nanoporous activated carbon derived from rice husk for environmental applications: kinetic and thermodynamic constants. Phys. Chem. Chem. Phys. **16**, 3924 (2014)

32. P. Thirukumaran, R. Atchudan, A. Shakila Parveen, Y.R. Lee, S.-C. Kim, The synthesis of mechanically stable polybenzoxazine-based porous carbon and its application as high-performance supercapacitor electrodes. New J. Chem. **45**, 8738 (2021)

33. P. Thirukumaran, R. Atchudan, A. Shakila Parveen, M. Santhamoorthy, V. Ramkumar, S.-C. Kim, N-doped mesoporous carbon prepared from a polybenzoxazine precursor for high performance supercapacitors. Polymers **13**, 2048 (2021)

34. B. Liu, X. Wang, Y. Chen, H. Xie, X. Zhao, A.B. Nassr, Y. Li, Honeycomb carbon obtained from coal liquefaction residual asphaltene for high-performance supercapacitors in ionic and organic liquid-based electrolytes. J. Energy Storage **68**, 107826 (2023)

35. R. Santhosh Kumar, P. Muthu Austeria, C. Sagaya Selvam Neethinathan, S. Ramakrishnan, K. Sekar, A.R. Kim, D.H. Kim, P.J. Yoo, D.J. Yoo, Highly mixed high-energy d-orbital states enhance oxygen evolution reactions in spinel catalysts. Appl. Surf. Sci. **641**, 158469 (2023)

36. M. Jalalah, S. Rudra, B. Aljafari, M. Irfan, S.S. Almasabi, T. Alsuwian, A.A. Patil, A.K. Nayak, F.A. Harraz, Novel porous heteroatom-doped biomass activated carbon nanoflakes for efficient solid-state symmetric supercapacitor devices. J. Taiwan Inst. Chem. Eng. **132**, 104148 (2022)

37. R. Atchudan, S. Perumal, D. Karthikeyan, A. Pandurangan, Y.R. Lee, Synthesis and characterization of graphitic mesoporous carbon using metal–metal oxide by chemical vapor deposition method. Microporous Mesoporous Mater. **215**, 123 (2015)

38. Y.X. Gan, Activated carbon from biomass sustainable sources. C **7**, 39 (2021)

39. I. Piñeiro-Prado, D. Salinas-Torres, R. Ruiz-Rosas, E. Morallón, D. Cazorla-Amorós, Design of activated carbon/activated carbon asymmetric capacitors. Front. Mater. (2016). https://doi.org/10.3389/fmats.2016.00016

40. K.S.W. Sing, Reporting physisorption data for gas/solid systems with special reference to the determination of surface area and porosity (recommendations 1984). Pure Appl. Chem. **57**, 603 (1985)

41. N.M. Musyoka, B.K. Mutuma, N. Manyala, Onion-derived activated carbons with enhanced surface area for improved hydrogen storage and electrochemical energy application. RSC Adv. **10**, 26928 (2020)

42. Z. Nie, Y. Huang, B. Ma, X. Qiu, N. Zhang, X. Xie, Z. Wu, Nitrogen-doped carbon with modulated surface chemistry and porous structure by a stepwise biomass activation process towards enhanced electrochemical lithium-ion storage. Sci. Rep. **9**, 15032 (2019)

43. M. Heckova, M. Streckova, R. Orinakova, J. Hovancova, A. Guboova, T. Sopcak, A. Kovalcikova, B. Plesingerova, D. Medved, J. Szabo, J. Dusza, Porous carbon fibers for effective hydrogen evolution. Appl. Surf. Sci. **506**, 144955 (2020)

44. T.N.J.I. Edison, R. Atchudan, M.G. Sethuraman, Y.R. Lee, Supercapacitor performance of carbon supported CO_3O_4 nanoparticles synthesized using *Terminalia chebula* fruit. J. Taiwan Inst. Chem. Eng. **68**, 489 (2016)

45. Y. Zheng, Y. Liu, X. Guo, Z. Chen, W. Zhang, Y. Wang, X. Tang, Y. Zhang, Y. Zhao, Sulfur-doped g-C_3N_4/rGO porous nanosheets for highly efficient photocatalytic degradation of refractory contaminants. J. Mater. Sci. Technol. **41**, 117 (2020)

46. S. Perumal, R. Atchudan, P. Thirukumaran, D.H. Yoon, Y.R. Lee, I.W. Cheong, Simultaneous removal of heavy metal ions using carbon dots-doped hydrogel particles. Chemosphere **286**, 131760 (2022)

47. R. Atchudan, T.N.J.I. Edison, D. Chakradhar, S. Perumal, J.-J. Shim, Y.R. Lee, Facile green synthesis of nitrogen-doped carbon dots using *Chionanthus retusus* fruit extract and investigation of their suitability for metal ion sensing and biological applications. Sens. Actuators, B Chem. **246**, 497 (2017)

48. X. Gao, L. Wu, W. Wan, Q. Xu, Z. Li, Preparation of activated carbons from walnut shell by fast activation with H_3PO_4: influence of fluidization of particles. Int. J. Chem. React. Eng. (2018). https://doi.org/10.1515/ijcre-2017-0074

49. A.A. Awe, B.O. Opeolu, O.S. Fatoki, O.S. Ayanda, V.A. Jackson, R. Snyman, Preparation and characterisation of activated carbon from *Vitis vinifera* leaf litter and its adsorption performance for aqueous phenanthrene. Appl. Biol. Chem. **63**, 12 (2020)

50. L. Shao, Y. Sang, N. Liu, J. Liu, P. Zhan, J. Huang, J. Chen, Selectable microporous carbons derived from poplar wood by three preparation routes for CO_2 capture. ACS Omega **5**, 17450 (2020)

51. W. Yang, Z. Du, Z. Ma, G. Wang, H. Bai, G. Shao, Facile synthesis of nitrogen-doped hierarchical porous lamellar carbon for high-performance supercapacitors. RSC Adv. **6**, 3942 (2016)

52. S. Karthikeyan, K. Ahmed, A. Osatiashtiani, A.F. Lee, K. Wilson, K. Sasaki, B. Coulson, W. Swansborough-Aston, R.E. Douthwaite, W. Li, Pompon dahlia-like Cu_2O/rGO nanostructures for visible light photocatalytic H_2 production and 4-chlorophenol degradation. ChemCatChem **12**, 1699 (2020)

53. S. Karthikeyan, D.D. Dionysiou, A.F. Lee, S. Suvitha, P. Maharaja, K. Wilson, G. Sekaran, Hydroxyl radical generation by cactus-like copper oxide nanoporous carbon catalysts for microcystin-LR environmental remediation. Catal. Sci. Technol. **6**, 530 (2016)

54. D. Shrestha, S. Maensiri, U. Wongpratat, S.W. Lee, A.R. Nyachhyon, *Shorea robusta* derived activated carbon decorated with manganese dioxide hybrid composite for improved capacitive behaviors. J. Environ. Chem. Eng. **7**, 103227 (2019)

55. A. Ilnicka, M. Skorupska, M. Tyc, K. Kowalska, P. Kamedulski, W. Zielinski, J.P. Lukaszewicz, Green algae and gelatine derived nitrogen rich carbon as an outstanding competitor to pt loaded carbon catalysts. Sci. Rep. **11**, 7084 (2021)

56. S. Perumal, R. Atchudan, T.N.J.I. Edison, J.-J. Shim, Y.R. Lee, Exfoliation and noncovalent functionalization of graphene surface with poly-n-vinyl-2-pyrrolidone by in situ polymerization. Molecules **26**, 1534 (2021)

57. T. Tang, M. Zhou, J. Lv, H. Cheng, H. Wang, D. Qin, G. Hu, X. Liu, Sensitive and selective electrochemical determination of uric acid in urine based on ultrasmall iron oxide nanoparticles decorated urchin-like nitrogen-doped carbon. Colloids Surf., B **216**, 112538 (2022)

58. L. Shi, L. Jin, Z. Meng, Y. Sun, C. Li, Y. Shen, A novel porous carbon material derived from the byproducts of bean curd stick manufacture for high-performance supercapacitor use. RSC Adv. **8**, 39937 (2018)

59. R. Chulliyote, H. Hareendrakrishnakumar, M. Raja, J.M. Gladis, A.M. Stephan, Sulfur-immobilized nitrogen and oxygen co-doped hierarchically porous biomass carbon for lithium–sulfur batteries:

influence of sulfur content and distribution on its performance. ChemistrySelect **2**, 10484 (2017)

60. P.M. Shanthi, P.J. Hanumantha, K. Ramalinga, B. Gattu, M.K. Datta, P.N. Kumta, Sulfonic acid based complex framework materials (CFM): nanostructured polysulfide immobilization systems for rechargeable lithium–sulfur battery. J. Electrochem. Soc. **166**, A1827 (2019)

61. H. He, Y. Zhang, W. Zhang, Y. Li, Y. Wang, P. Wang, D. Hu, Dual metal-loaded porous carbon materials derived from silk fibroin as bifunctional electrocatalysts for hydrogen evolution reaction and oxygen evolution reaction. ACS Appl. Mater. Interfaces. **13**, 30678 (2021)

62. Z. Wu, M. Song, Z. Zhang, J. Wang, H. Wang, X. Liu, Porous two-dimensional layerd molybdenum compounds coupled with n-doped carbon based electrocatalysts for hydrogen evolution reaction. Appl. Surf. Sci. **465**, 724 (2019)

63. G. Han, M. Hu, Y. Liu, J. Gao, L. Han, S. Lu, H. Cao, X. Wu, B. Li, Efficient carbon-based catalyst derived from natural cattail fiber for hydrogen evolution reaction. J. Solid State Chem. **274**, 207 (2019)

64. V.C. Hoang, V.G. Gomes, K.N. Dinh, Ni- and p-doped carbon from waste biomass: a sustainable multifunctional electrode for oxygen reduction, oxygen evolution and hydrogen evolution reactions. Electrochim. Acta **314**, 49 (2019)

65. D.N. Sangeetha, D. Krishna Bhat, S. Senthil Kumar, M. Selvakumar, Improving hydrogen evolution reaction and capacitive

properties on CoS/MoS$_2$ decorated carbon fibers. Int. J. Hydrogen Energy **45**, 7788 (2020)

66. A. Kahyarian, B. Brown, S. Nesic, Mechanism of the hydrogen evolution reaction in mildly acidic environments on gold. J. Electrochem. Soc. **164**, H365 (2017)

67. R. Atchudan, S. Perumal, T.N. Jebakumar Immanuel Edison, S. Aldawood, R. Vinodh, A.K. Sundramoorthy, G. Ghodake, Y.R. Lee, Facile synthesis of novel molybdenum disulfide decorated banana peel porous carbon electrode for hydrogen evolution reaction. Chemosphere **307**, 135712 (2022)

68. G. Hou, J. Wu, T. Li, J. Lin, B. Wang, L. Peng, T. Yan, L. Hao, L. Qiao, X. Wu, Nitrogen-rich biomass derived three-dimensional porous structure captures feni metal nanospheres: an effective electrocatalyst for oxygen evolution reaction. Int. J. Hydrogen Energy **47**, 12487 (2022)